

Supplementary information

Selective Oxidative of Polyols to Primary hydroxyl acids by Plasmonic Catalysis on Au-Pt Nanoalloy Irradiated by Visible Light

Zishuai Wang,^a Yaoqiang Wang,^a Gang Xiao,^{*a} Yu Jin and Haijia Su^{*a}

a. Beijing Key Laboratory of Bioprocess, College of Life Science and Technology, Beijing University of Chemical Technology, Beijing 100029, China.

E-mail: sewicxiao@hotmail.com, xiaogang@mail.buct.edu.cn (G. Xiao); suhj@mail.buct.edu.cn (H. Su).

Materials and Chemicals

Zirconium dioxide (ZrO_2 , 99.99%, 50nm), Chloroplatinic acid hydrate ($\text{H}_2\text{Cl}_6\text{Pt}\cdot x\text{H}_2\text{O}$, $\geq 99.95\%$ trace metal basis) and gold chloride trihydrate ($\text{HAuCl}_4\cdot 3\text{H}_2\text{O}$, $\geq 99.9\%$ trace metal basis) were purchased from Aladdin (Shanghai, China). Ethylene glycol (EG, $\geq 99.5\%$), sodium borohydride (NaBH_4 , $\geq 98.0\%$), glycolic acid (GA, $\geq 98\%$), Glycerol ($\geq 99\%$), 1,2-butanediol ($\geq 98\%$), 2,3-Dihydroxypropanoic acid ($\geq 95\%$, 20% in water), and 2-Hydroxybutyric acid ($\geq 95\%$) were purchased from Macklin (Shanghai, China).

All the chemicals and materials were used as received without further purification. Deionized water was used throughout the experiments.

Catalysts preparation

ZrO_2 supported Au-Pt alloy nanoparticles with different Au-Pt mass ratios were synthesized by the impregnation-reduction method reported in our previous work.¹ In a typical procedure of preparing Au-Pt/ ZrO_2 (Au=1.875 wt.%, Pt=1.125 wt.%), 0.5 g ZrO_2 powder, 3mL of 0.01 M H_2PtCl_6 and 5 mL of 0.01 M HAuCl_4 was dispersed into 350 mL ethanol with 15min sonication and another 20 min magnetically stirring at room temperature. Then 16 mL of 0.01M NaBH_4 aqueous solution was added drip by drip in 30 min, stirred for 2 h and aging overnight. The solid was collected and washed with ethanol three times, followed by drying in a vacuum oven at 40 °C overnight. Au-Pt/ ZrO_2 with different Au-Pt mass ratios were prepared using the same procedure but varying the volume of H_2PtCl_6 or HAuCl_4 . Au/ ZrO_2 or Pt/ ZrO_2 were prepared in the same way by using HAuCl_4 or H_2PtCl_6 as the metal precursor.

General procedure for polyols oxidation photocatalytic reactions

Unless otherwise specified, all the photocatalytic reactions were performed in a 20 mL quartz tube (diameter = 16 mm) on a ten-cell photocatalytic reactor (WATTCAS, WP-TEC-1020HSL). During the photocatalytic reaction, the reaction mixture was irradiated by LED light source (visible light, spectral output in the range of 400-800 nm, Fig. S1), and the temperature was precisely controlled using a circulating water bath. Dark reactions were also conducted in the same photocatalytic reactor without light illumination. In the light intensity study, the light source was a white LED lamp and the light intensity range is 90-310 $\text{mW}\cdot\text{cm}^{-2}$ (Fig. 2a). In the wavelength dependence study, the wavelength of light are 365nm, 412nm, 512nm, 598nm, and 702nm (Fig. 2b). Gram-scale photocatalytic reaction was conducted in a batch reactor (Fig. S2) and a continuous-flow reactor (Fig. S3). All the reactions were conducted in triplicate to obtain reproducible results.

After the reaction, the reaction solution was collected and filtered through a filter (pore size 0.22 μm)

to remove the solid catalyst. The liquid products were analyzed by high performance liquid chromatography (HPLC, Agilent 1260 Infinity II) equipped with UV detector, refractive index (RID) and organic acid analysis column (AMINEX HPX-87H). For the HPLC analysis, the UV detector was set at 210 nm, the mobile phase was 5 mM H₂SO₄ at a flow rate of 0.5 mL/min. The polyols conversion (X), primary hydroxyl acids selectivity (S) and primary hydroxyl acids yield (Y) were calculated as follows:

$$X(\%) = \frac{C_0 - C_t}{C_0} \times 100\%$$

$$S(\%) = \frac{K_t}{C_0 - C_t} \times 100\%$$

$$Y(\%) = \frac{K_t}{C_0} \times 100\%$$

C_0 (mol/L) is the initial concentration of polyols (mol/L), C_t (mol/L) is the concentration of polyols after specific reaction time, and K_t (mol/L) is the concentration of primary hydroxyl acids after the reaction.

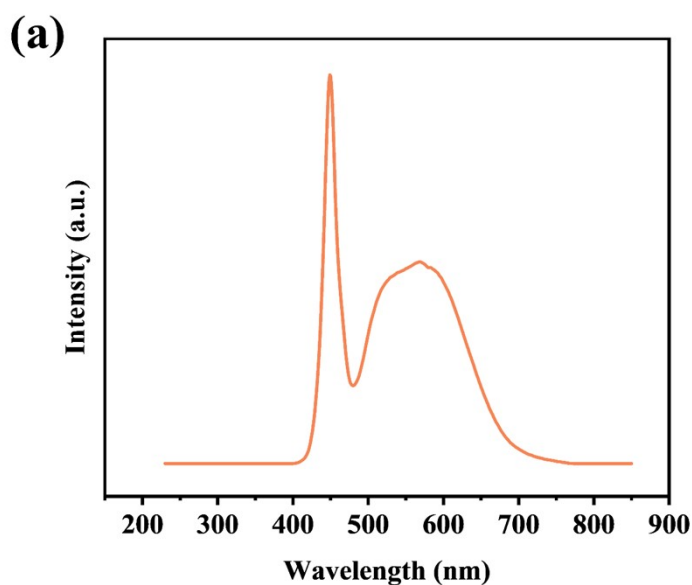


Fig. S1 (a) The output spectral distribution of the white LED lamp. (b) Photographs of experimental setup.

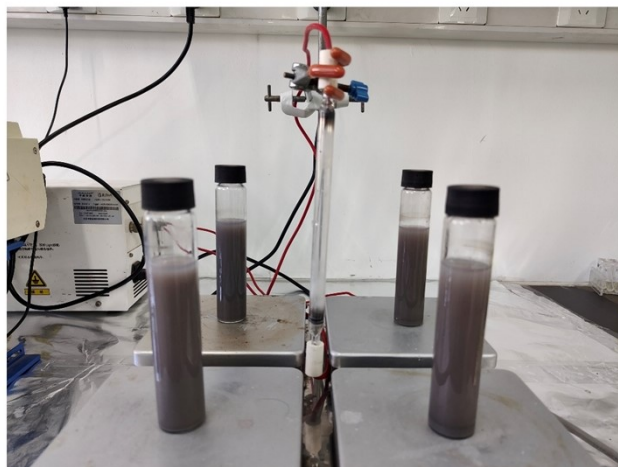


Fig. S2 Experimental setup for batch reactor system.

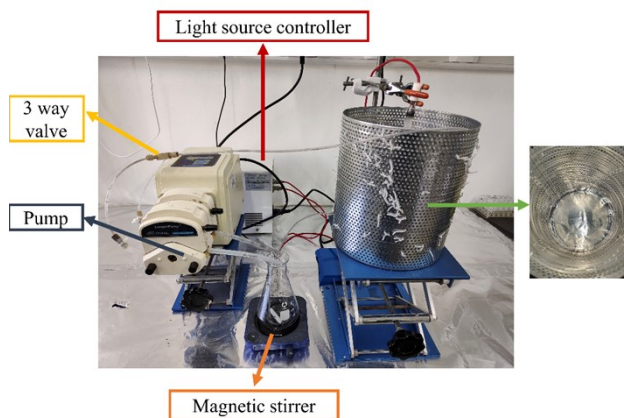


Fig. S3 Experimental setup for continuous-flow reactor system.

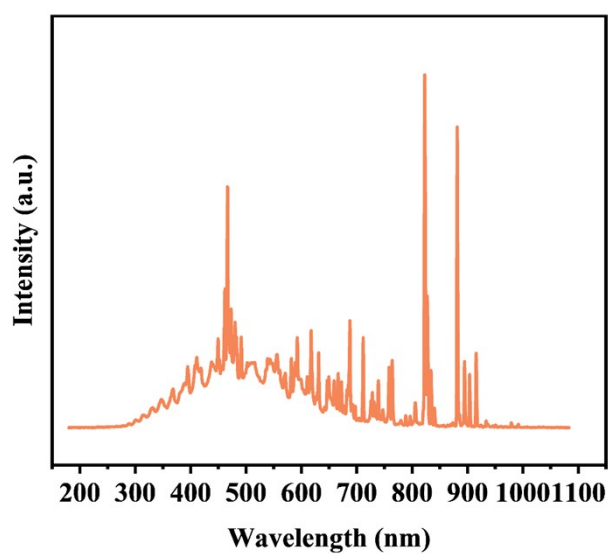


Fig. S4 (a) The output spectral distribution of the Xe lamp used in batch reactor and continuous-flow reactor.

Product separation and purification from continuous-flow reactor system

KOH was added to the reacted solution for the formation of glycolate product. Typical, the post-reaction solution was evaporated to remove water, which precipitates both glycolate and excess KOH from the unreacted EG. Ethanol was then added to separate the glycolate from the precipitate, as glycolate has poor solubility in ethanol while KOH dissolves well in ethanol. The final product is obtained in the form of glycolate.

PET hydrolysis process

0.3 g commercial PET was added into 30 mL 0.5 M KOH aqueous solution, which was subsequently transferred to 50 mL Teflon-lined autoclave and then kept at 180 °C for 12 h. The concentration of EG in hydrolysate was 0.05 M, and the hydrolysate was used for further oxidation process.

E-factor (Scheme 1)

The E-factor calculated according to the following equation.

$$\text{E-factor} = \frac{m_{\text{waste}}}{m_{\text{primary hydroxyl acids}}}$$

$$m_{\text{primary hydroxyl acids}} = n_{\text{polyols}} \times \text{yield} \times \text{MW}_{\text{primary hydroxyl acids}}$$

$$m_{\text{waste}} = n_{\text{polyols}} + n_{\text{oxidizing agent}} - m_{\text{primary hydroxyl acids}} + m_{\text{KOH/NaOH}}$$

Molar ratio of waste/primary hydroxyl acids (Scheme 1)

The molar ratio of waste (byproducts and KOH or NaOH)/primary hydroxyl acids was calculated according to the following equation.

$$\text{Molar ratio of waste/primary hydroxyl acids} = \frac{n_{\text{waste}}}{n_{\text{primary hydroxyl acids}}}$$

$$n_{\text{waste}} = n_{\text{polyols}} \times (1 - \text{yield}) + n_{\text{KOH/NaOH}}$$

$$n_{\text{primary hydroxyl acids}} = n_{\text{polyols}} \times \text{yield}$$

The primary hydroxyl acids yield was collected from references in Scheme 1.

Energy Consumption

For the light reaction:

$$(650 \text{ W (stirrer)} + 10 \text{ W (light)}) \times 12 \text{ h} = 7.92 \text{ kW} \cdot \text{h} = 28512 \text{ kJ}$$

$$28512 \text{ kJ} / 76.85 \text{ mmol GA} = 371 \text{ kJ/mmol GA}$$

For the dark reaction:

$$650 \text{ W (stirrer)} \times 12 \text{ h} = 7.8 \text{ kW} \cdot \text{h} = 28080 \text{ kJ}$$

$$28080 \text{ kJ} / 15.78 \text{ mmol GA} = 1779 \text{ kJ/mmol GA}$$

Catalysts characterization

The morphology and structure of the catalysts were characterized on a high-resolution transmission electron microscopy (TEM, JEM-2100F) with an acceleration voltage of 200 kV and on a high-angle

annular dark-field scanning TEM. Powder X-Ray Diffraction (XRD) was obtained on a Rigaku SmartLab SE diffractometer using Cu K α radiation. The absorption spectra of catalysts were collected on a UV-3150 UV-Vis spectrophotometer equipped with an integrating sphere using BaSO₄ as the reference. Photoluminescence (PL) spectra were measured using a fluorescence life time spectrometer (Edinburgh FLS1000). The electrochemical impedance spectroscopy (EIS) of the catalysts were recorded on a RST5000 electrochemical station. The photocurrent properties and cyclic voltammetry curves were studied on a CHI760E electrochemical station. A standard three-electrode system using a platinum plate as the counter electrode, Ag/AgCl electrode as the reference electrode, and FTO glass coated with samples as the working electrode, and a solution of 0.1 mol/L sodium sulfate (Na₂SO₄) as the electrolyte was prepared for the tests. The working electrode was prepared as follows: 1 mg of the catalysts were first mixed with 400 μ L ethanol, 125 μ L water, and 50 μ L Nafion, then the slurry was coated on to FTO electrodes. The obtained electrodes were dried at 60 °C before the test. *In-situ* Xray photoelectron spectroscopy (XPS) measurement were recorded by PHI versoprobe 5000III under illumination or dark condition. *In-situ* Fourier transform infrared spectroscopy (FTIR) spectra were collected using the Thermo Scientific Nicolet iS50 spectrometer equipped with an in situ diffuse reflectance cell (Harrick).

Computational method

We have employed the Vienna Ab initio Simulation Package (VASP) to perform all density functional theory (DFT) calculations within the generalized gradient approximation (GGA) using the Revised Perdew-Burke-Ernzerhof (r-PBE) functional. We have chosen the projected augmented wave (PAW) potentials to describe the ionic cores and take valence electrons into account using a plane wave basis set with a kinetic energy cutoff of 450 eV. The DFT-D3 empirical correction method was employed to describe van der Waals interactions. Geometry optimizations were performed with the force convergence smaller than 0.05 eV/Å. The convergence accuracy for the energy is 10⁻⁵ eV. Four-layer 6 \times 6 supercell was constructed for (111) surface of Au and Pt. AuPt (111) is a surface alloy, surface metal atoms Au: Pt = 2:1. Monkhorst-Pack k-points of 1 \times 1 \times 1 was applied for all the calculations. Half atoms at bottom are fixed in all the calculations. The adsorption energy (E_a) is calculated by the equation:

$$E_a = E(\text{slab} + \text{C}_2\text{H}_4\text{O}_3) - E(\text{slab}) - E(\text{C}_2\text{H}_4\text{O}_3).$$

$$E_a = E(\text{slab} + \text{C}_2\text{H}_6\text{O}_2) - E(\text{slab}) - E(\text{C}_2\text{H}_6\text{O}_2).$$

$$E_a = E(\text{slab} + \text{O}_2) - E(\text{slab}) - E(\text{O}_2).$$

where $E(\text{slab} + \text{C}_2\text{H}_4\text{O}_3/\text{C}_2\text{H}_6\text{O}_2/\text{O}_2)$ and $E(\text{slab})$ are the total energy of the surface slab with and without $\text{C}_2\text{H}_4\text{O}_3/\text{C}_2\text{H}_6\text{O}_2/\text{O}_2$ -adsorption, respectively, and $E(\text{C}_2\text{H}_4\text{O}_3/\text{C}_2\text{H}_6\text{O}_2/\text{O}_2)$ is the total energy of the

C₂H₄O₃/C₂H₆O₂/O₂ molecule in the gas phase.

According to the *in-situ* XPS results, the adsorption energy of O₂ on Au-Pt/ZrO₂ was calculated in electron-rich state.

Lattice parameter:

Au(111) and AuPt(111): a = b = 17.30 Å c = 22.06 Å, α = 90° β = 90°, γ = 120°.

Pt(111): a = b = 16.65 Å c = 21.80 Å, α = 90° β = 90°, γ = 120°.

Adsorption experiments of EG

The adsorption experiments of EG on catalysts in the dark and under light irradiation were conducted under an argon atmosphere to prevent oxidation reaction. The initial concentration used in adsorption experiments was 0.01M and much lower than that used in the oxidation reaction.

$$\text{Concentration change (\%)} = \frac{C_0 - C_t}{C_t} \times 100\%$$

Finite-difference time-domain (FDTD) simulations

FDTD simulations were conducted to describe the spatial local electric field of different catalysts caused by LSPR. The simulated sizes and shapes of Au/ZrO₂, Pt/ZrO₂ and Au/Pt-ZrO₂ were determined according to the TEM images. We use the numerical simulation software FDTD based on Maxwell equations to solve the electric field distribution of nanostructures. We set the x, y, and z directions to perfectly match the layer conditions, which are set to prevent non-physical reflections. When a plane wave is vertically incident on the nanostructure along the z direction, we use an electric field monitor to monitor the electric field distribution in the x-y plane. In addition, we divided the entire simulation region into a mesh of 0.25nm*0.25nm*0.25nm, which is to ensure that the calculation results are accurate and reliable.

Table. S1 EG oxidation by photoelectrocatalysis or the photoreforming system in recent literatures

Catalyst	Reaction conditions	Products	Ref
Pt-CdS/N-GQDs	EG 1 M, 1 M KOH, visible light 200 mW·cm ⁻²	CO ₂ H ₂ O	2
PdCu	EG 1 M, 1 M KOH, Xe lamp 150 W	CO ₂ H ₂ O	3
PdAgCu	EG 1 M, 1 M KOH, Xe lamp 150 W	CO ₂ H ₂ O	4

Table. S2 Productivity of different catalyst in polyols oxidation system

Reagent	Catalyst	Productivity/ (mmol primary hydroxyl acids/ g catalyst/ h)	Ref
Ethylene glycol	[Cp*Ir(bpyO)]OH ⁻	3.74	5
	Pt-Fe/ZrO ₂	44.95	6
	Pt/HAP	58.425	7
	Pt/Mn ₂ O ₃	4.05	8
	Au-Pt/ZrO ₂	0.64/2.02(continuous-flow reactor)	Our work
Glycerol	Pt/ZrO ₂	3.02	9
	Pt/Cu-CuZrOX	21.66	10
	Au-Pt/TiO ₂	1.74	11
	Pt@TiOX	5.14	12
	Pt/TiO ₂	3.40	13
	Pt-Cu/C	4.92	14
	Au-Pt/ZrO ₂	0.58/1.62(continuous-flow reactor)	Our work

Table. S3 ICP-MS analysis of the catalysts

Au:Pt Weight ratio	Au wt.%	Pt wt.%
0:3		2.564
0.75:2.25	0.670	1.524
1.125:1.875	1.058	1.361
1.5:1.5	1.429	1.119
1.875:1.125	1.795	0.861
2.25:0.75	2.032	0.533
2.625:0.375	2.586	0.289
3:0	2.765	

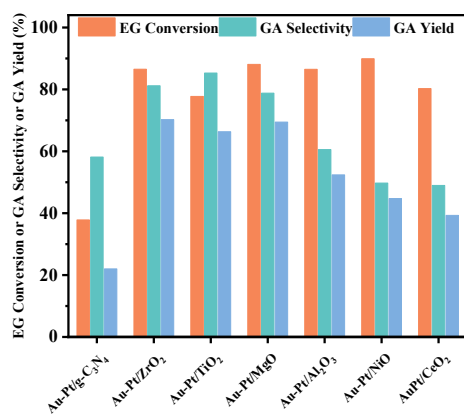


Fig. S5 Photocatalytic performance for the selective oxidation of EG under visible light catalyzed by different catalysts. Reaction conditions: EG (50 mM, 2 mL H₂O), 10 mg of photocatalyst, air atmosphere (1 atm), 40 °C, 8 h, 300 mW·cm⁻² intensity of visible light.

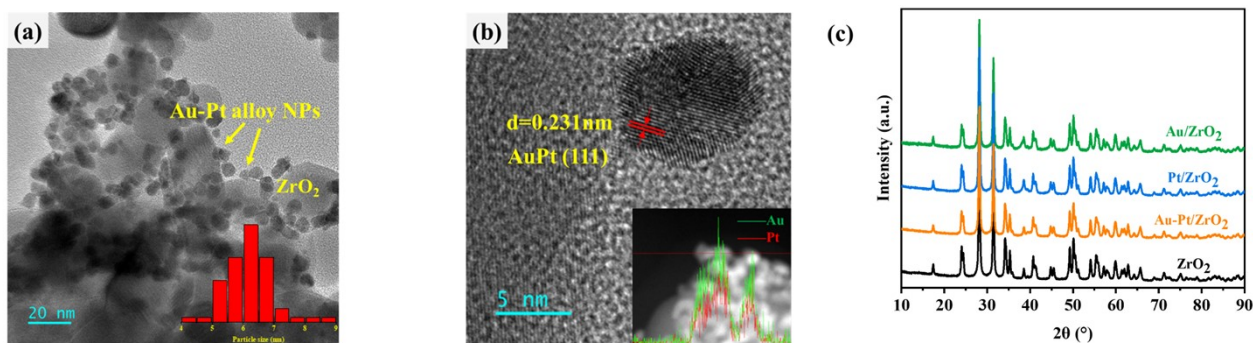


Fig. S6 Characterization of Au-Pt/ZrO₂: (a) TEM images of Au-Pt alloy nanoparticles supported by ZrO₂, (b) high resolution TEM image of a typical Au-Pt alloy nanoparticle, (c) XRD patterns of Au/ZrO₂, Pt/ZrO₂, Au-Pt/ZrO₂ and ZrO₂.

We characterized the Au-Pt/ZrO₂ catalysts by transmission electron microscopy (TEM) and energy-dispersive X-ray spectroscopy (EDX) to study the morphology and composition. The average diameter of Au-Pt nanoalloy was determined to be 6.2 nm. The high-resolution TEM image shows that the lattice fringe distance is 0.231 nm, which can be assigned to be the (111) planes of face-centered cubic AuPt nanoalloys.¹⁵ The EDX line profiles of Au and Pt shows that Au and Pt are mixed homogeneously in the nanoparticles. These results further proved that the formation of AuPt alloy structure. From the X-Ray Diffraction (XRD) analysis results, no related peaks assigned to Au or Pt is identified due to the small particle sizes and low metal loadings. The XRD patterns also show that the formation of nanoparticles did not lead to the incorporation of impurities.

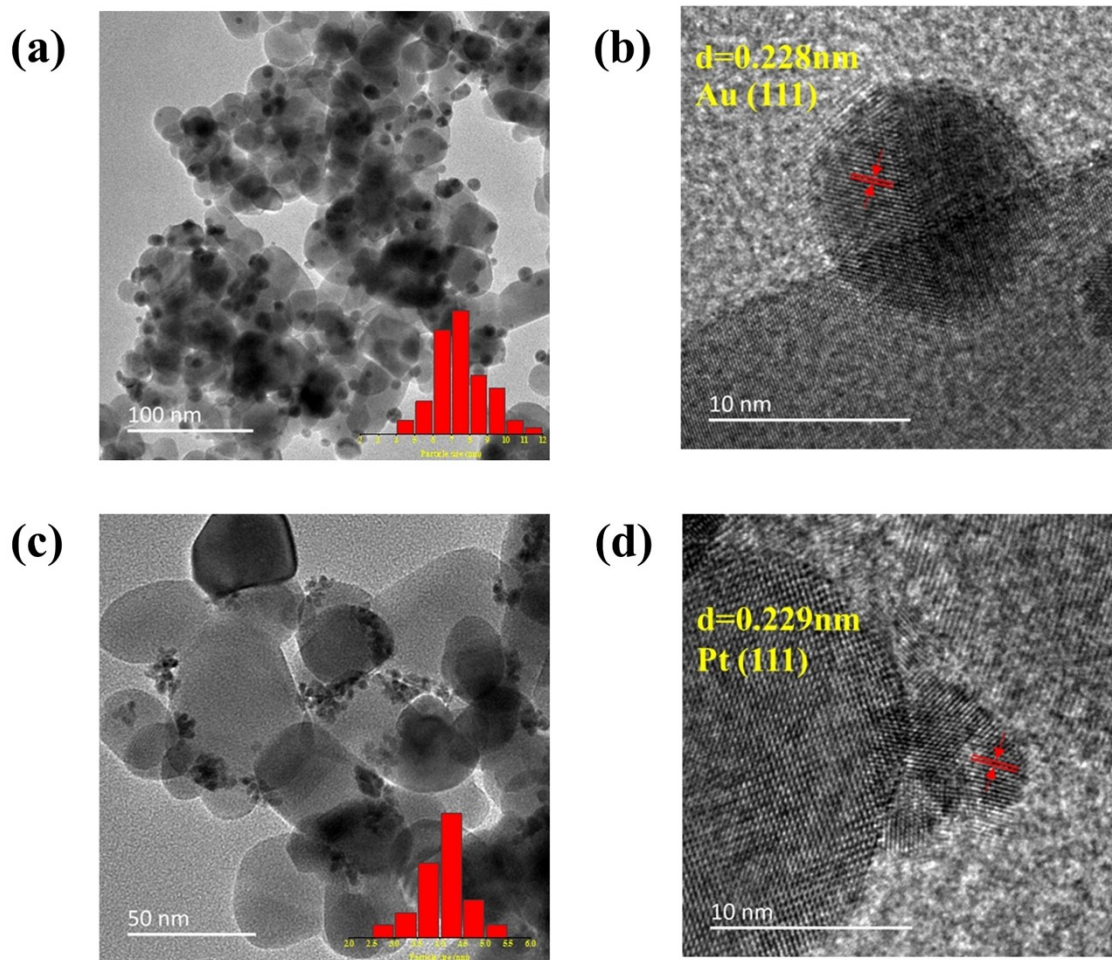


Fig. S7 (a-b) TEM images of Au/ZrO₂ nanoparticles; (c-d) TEM images of Pt/ZrO₂ nanoparticles

The average diameter of Au/ZrO₂ and Pt/ZrO₂ was $7.51\pm 1.4\text{nm}$ and $4.07\pm 0.5\text{nm}$ respectively. The high-resolution TEM images show that the lattice fringe distance of Au and Pt is 0.228 nm and 0.229 nm, respectively, which can be assigned to be the (111) planes of face-centered cubic Au and Pt nanoparticles.¹⁶⁻¹⁸ The information was used for DFT calculation and FDTD simulations.

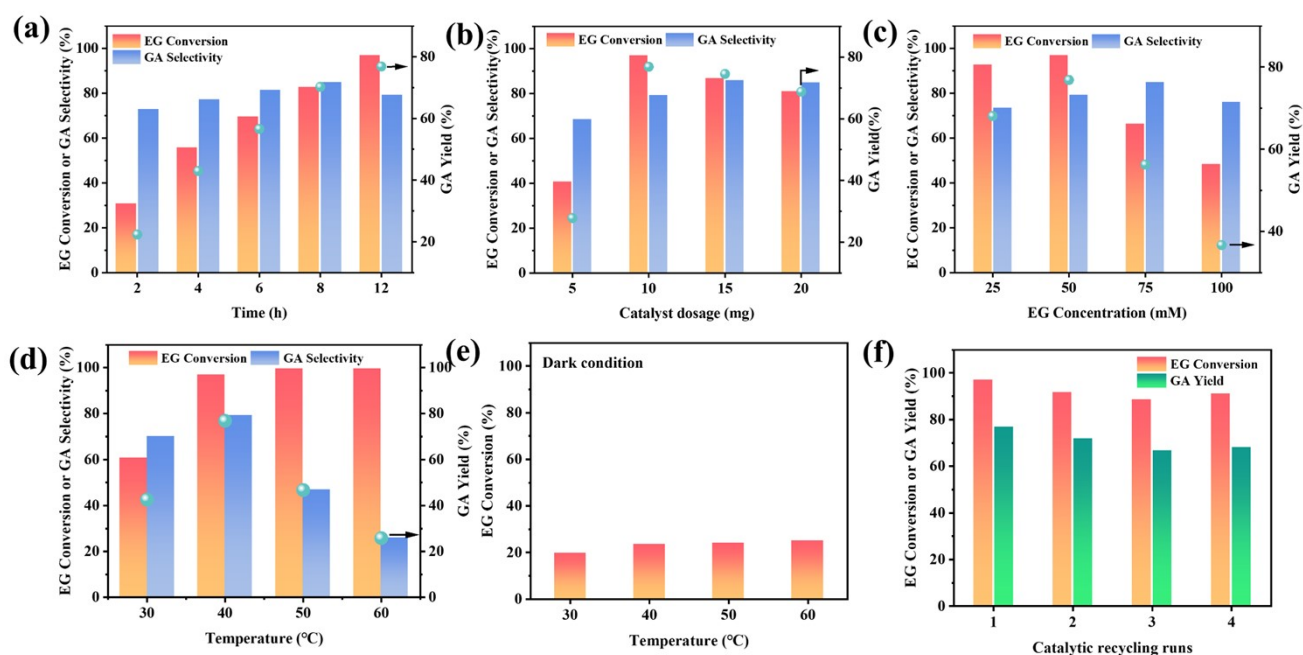
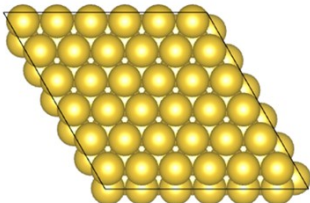
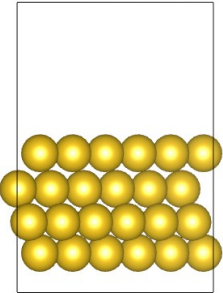
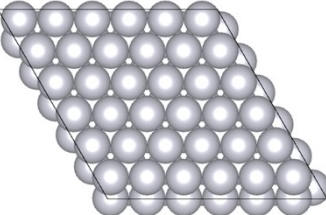
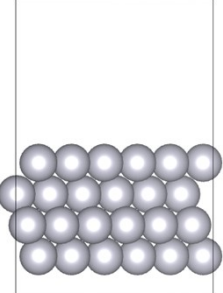
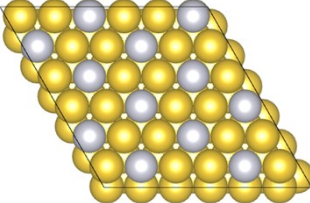
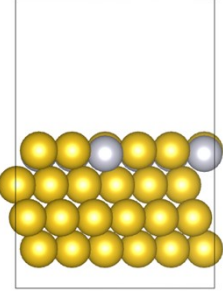


Fig. S8 The effects of (a) reaction time, (b) catalyst dosage, (c) EG concentration, (d) reaction temperature on the photocatalytic oxidation of EG to GA on Au-Pt/ZrO₂. (e) The thermal effect of EG conversion in dark condition. (f) The recycling experiments of Au-Pt/ZrO₂ for EG oxidation. Standard reaction conditions: EG (50 mM, 2 mL H₂O), 10 mg of photocatalyst, air atmosphere (1 atm), 40 °C, 12h, 300 mW·cm⁻² intensity of visible light.

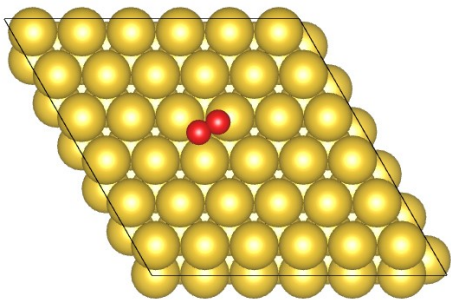
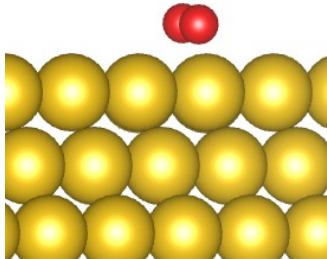
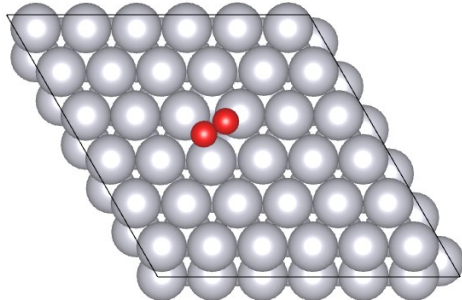
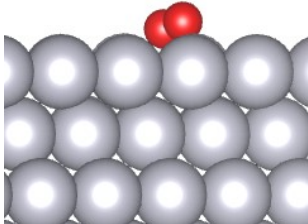
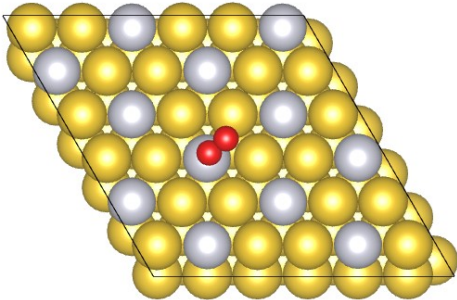
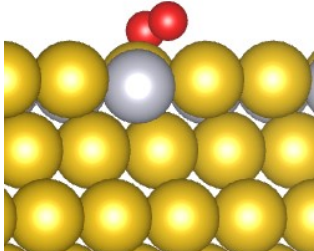
The performance of Au-Pt/ZrO₂ for EG photocatalytic oxidation of EG was investigated. When the reaction time was prolonged to 12 h, the EG conversion can be higher than 95%. The selectivity of GA increased to 84.9% in 8 h, and then decreased slightly. Fig. S8 (b) shows the effect of catalyst dosage on the photocatalytic oxidation of EG. When the catalyst dosage was increased from 5 mg to 10 mg, the EG conversion and GA yield increased to the maximum value. However, due to the high catalyst dosage led to the underutilization of light, the EG conversion and GA yield decreased slightly when the catalyst dosage was further increased from 10 mg to 20 mg. The highest GA yield was obtained under 50 mM initial EG concentration. Fig. S8 (d) clearly shows that the conversion of EG increases from 60.7% to nearly 100% with the temperature increasing from 30 °C to 60 °C. On the other hand, a 30 °C increase of reaction temperature cannot promote the EG oxidation in the dark, and the EG conversion is still below 25%. Then the recycling experiments was studied. The EG conversion and GA yield under visible light was well preserved during four cycles.

Table. S4 Top and side views of Au(111), Pt (111) and AuPt(111) slab model

	Top View	Side View
Au/ZrO ₂		
Pt/ZrO ₂		
Au-Pt/ZrO ₂		

Au (golden), C (grey), O (red), H (white)

Table. S5 Top and side views of O₂ adsorption model for Au/ZrO₂, Pt/ZrO₂ and Au-Pt/ZrO₂

	Top View	Side View
Au/ZrO ₂		
Pt/ZrO ₂		
Au-Pt/ZrO ₂		

Au (golden), C (grey), O (red), H (white)

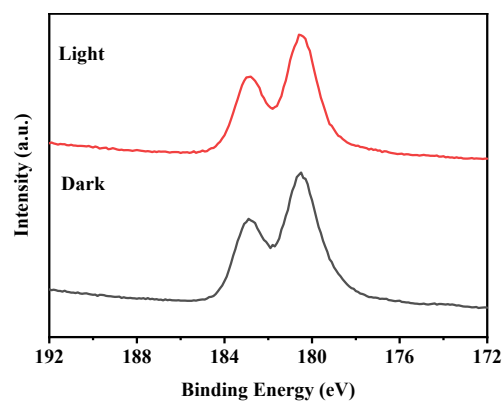


Fig. S9 In-situ high-resolution XPS spectra of Zr 3d under dark and light condition.

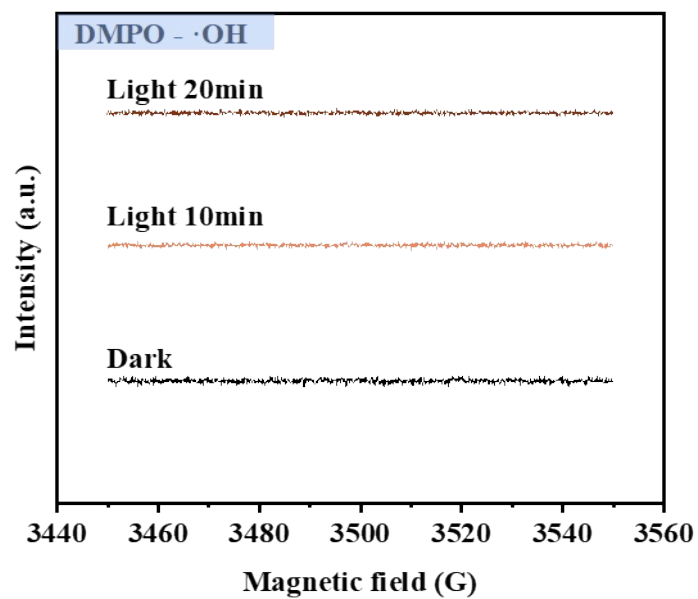


Fig. S10 EPR spectra of Au-Pt/ZrO₂ in the presence of DMPO (a spin-trapping agent) with or without light irradiation.

Table. S6 Influence of the additive on the photocatalytic performance.

Reactant	Additive	Conversion/%	Yield of acids/%
EG	/	69.51	56.61
EG	isopropanol	65.31	51.93

Reaction conditions: EG (50 mM, 2 mL H₂O), 10 mg of photocatalyst, air atmosphere (1 atm), 40 °C, 6h. Isopropanol act as hole scavengers.

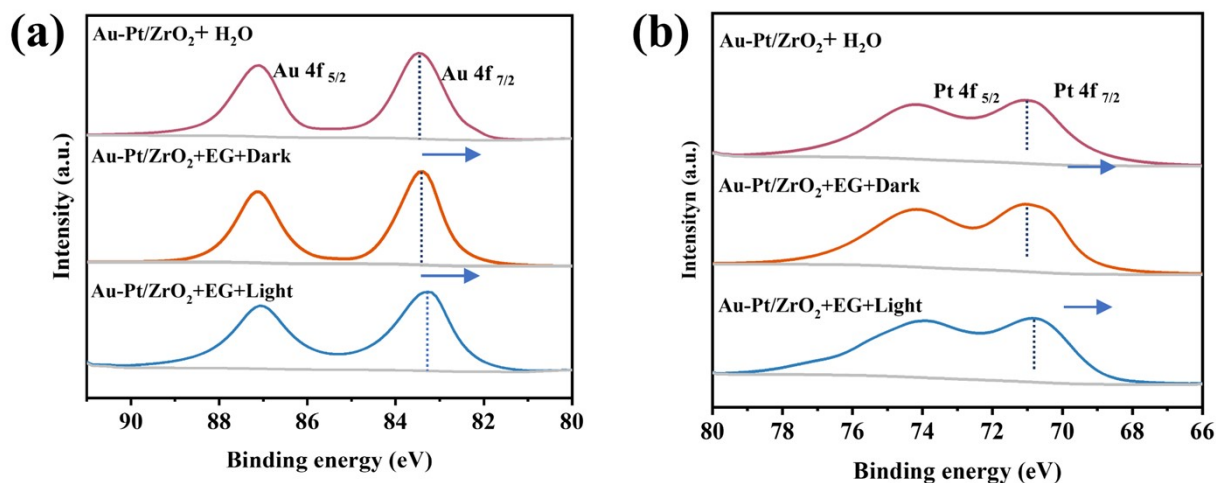


Fig. S11 XPS spectra of Au-Pt/ZrO₂ after 2h of light reaction with and without light.

The strong adsorption of the EG compound onto the catalyst surface induces a negative shift in the binding energy of both Au and Pt, as illustrated in Fig. S11 a-b. The light-promoted adsorption of Au-Pt/ZrO₂ towards EG is identified as a contributing factor to the significant enhancement of EG oxidation ability under light conditions in comparison to the dark condition.

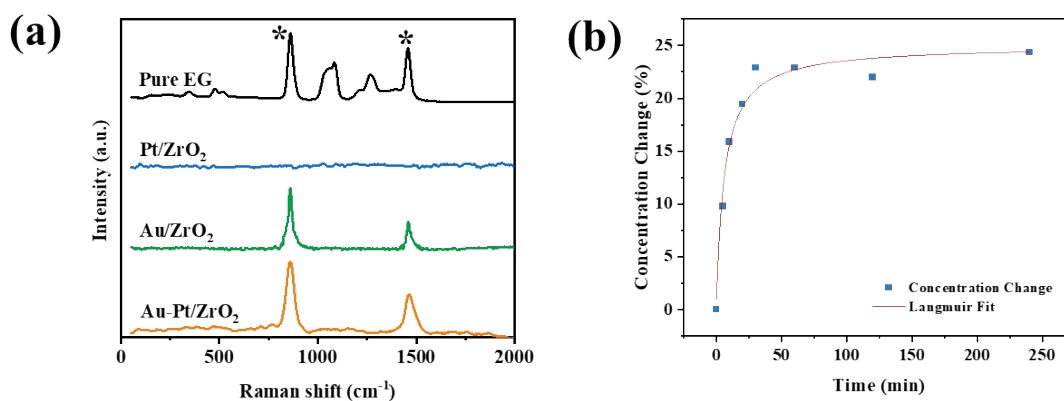


Fig. S12 (a) Surface Enhanced Raman spectra of EG adsorbed on the catalysts of Au/ZrO₂, Pt/ZrO₂ and Au-Pt/ZrO₂. The characteristic vibrations of the EG are marked with “*” (b) The EG concentration change caused by adsorption under light and Langmuir fit curve.

The intensified EM fields significantly influence the properties of molecules within them. It is widely acknowledged that the driving force behind Surface-Enhanced Raman Scattering (SERS) primarily stems from the amplification of EM fields due to the excitation of surface plasmon resonance.¹⁹ The SERS intensity is approximately positively related to the EM field intensity. The findings indicate that upon the absorption of EG onto the Au-Pt/ZrO₂ catalyst, SERS peaks manifest significantly heightened intensity

in comparison to the relatively weak SERS peaks of EG adsorbed on Au/ZrO₂. Notably, no SERS signals were detected with Pt/ZrO₂. We further did the adsorption experiments and the adsorption fitted the Langmuir-Hinshelwood model.

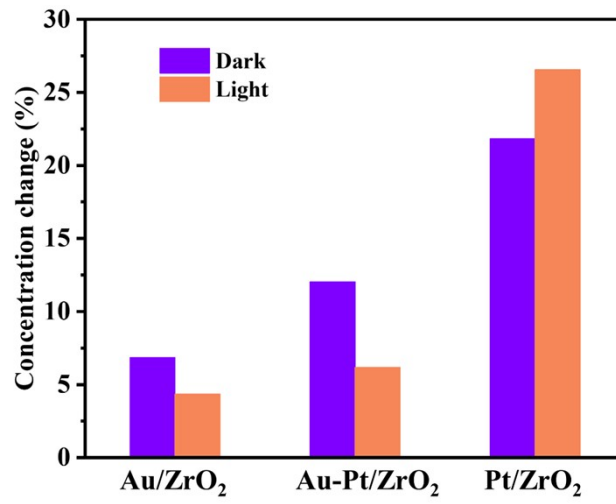


Fig. S13 The GA concentration change caused by adsorption under light and in the dark

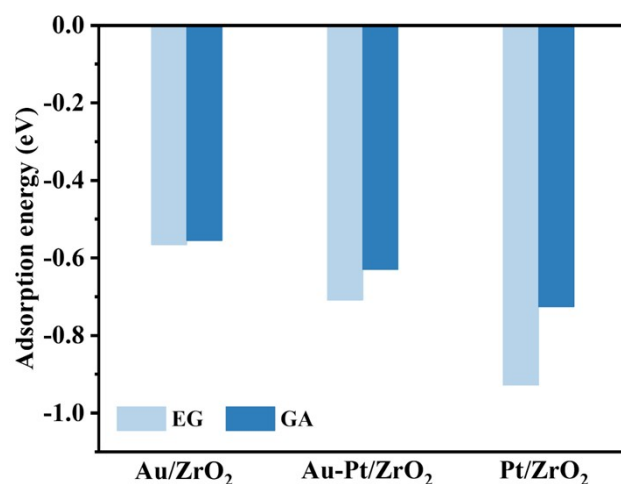
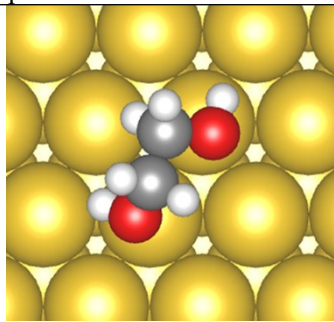
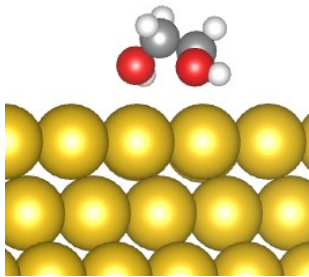
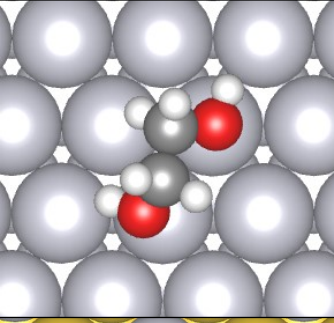
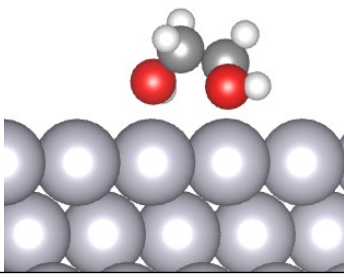
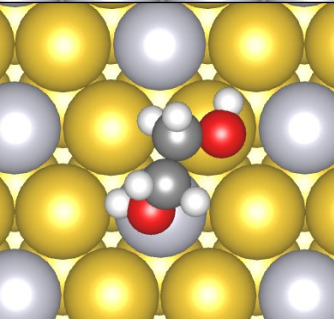
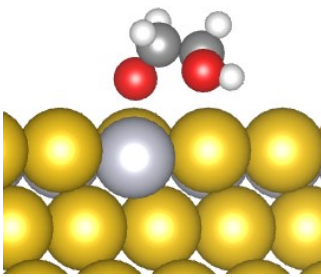


Fig. S14 Adsorption energy of EG and GA on Au/ZrO₂, Pt/ZrO₂, Au-Pt/ZrO₂

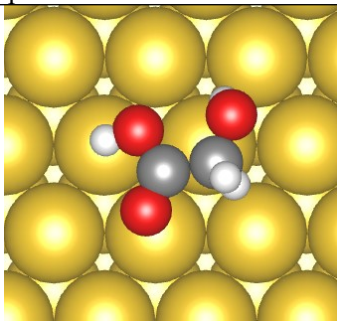
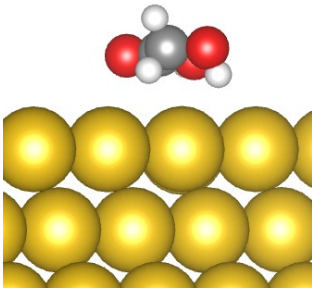
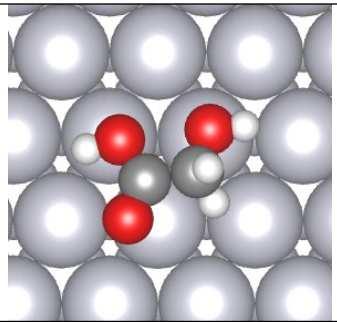
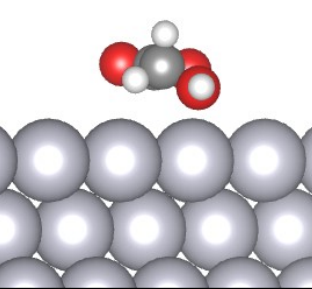
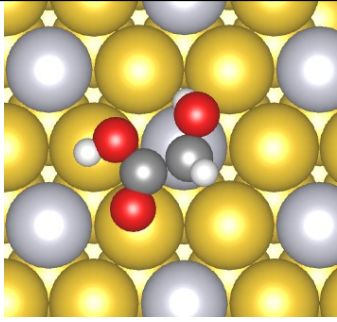
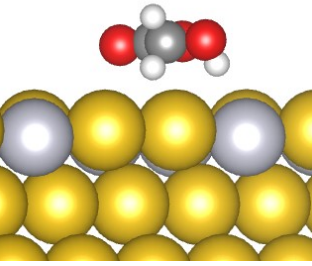
The adsorption energy of EG and GA on Au/ZrO₂, Pt/ZrO₂ and Au-Pt/ZrO₂ were summarized in Fig.S13. Obviously, the adsorption energy of EG and GA on Pt/ZrO₂ surpassed that on Au/ZrO₂ and Au-Pt/ZrO₂. However, the intensity of EM fields of Pt/ZrO₂ is too relatively weak to affect the adsorption properties (Fig. 4a). The order of the GA adsorption energy is also consistent with the selectivity in the absence of light condition showed in Fig. 1a. The above results indicate that Au-Pt/ZrO₂ could not only exhibits an increased adsorption capacity for EG molecules but also improves the GA selectivity under the influenced of LSPR-induced high EM field intensity.

Table. S7 Top and side views of EG adsorption model for Au/ZrO₂, Pt/ZrO₂ and Au-Pt/ZrO₂

	Top View	Side View
Au/ZrO ₂		
Pt/ZrO ₂		
Au-Pt/ZrO ₂		

Au (golden), C (grey), O (red), H (white)

Table. S8 Top and side views of GA adsorption model for Au/ZrO₂, Pt/ZrO₂ and Au-Pt/ZrO₂

	Top View	Side View
Au/ZrO ₂		
Pt/ZrO ₂		
Au-Pt/ZrO ₂		

Au (golden), C (grey), O (red), H (white)

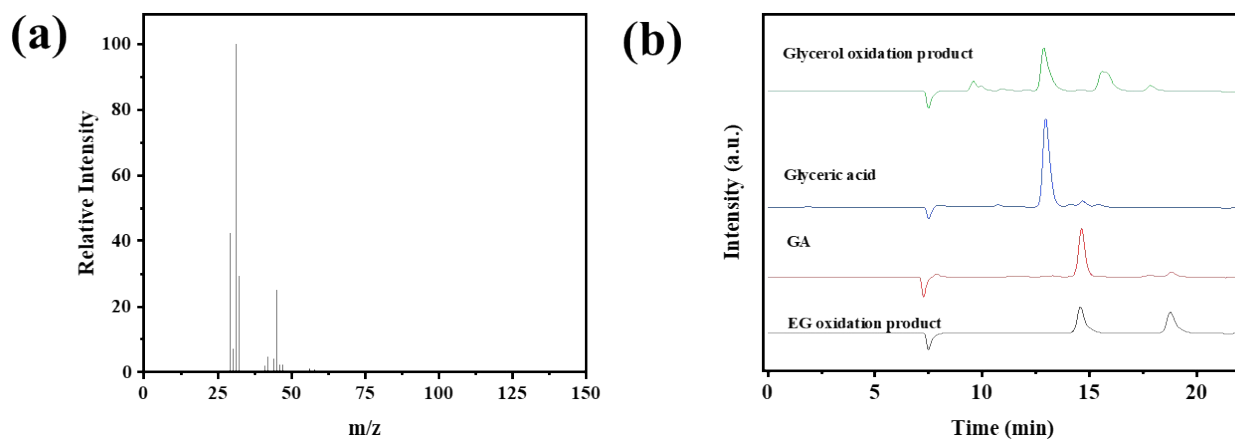


Fig. S15 (a) Gas chromatography–mass spectrometry of main product from EG oxidation. (b)HPLC results with RID detector of reaction solutions and standard chemicals

References

- 1 G. Xiao, Y. wang, Y. Zhao, P. Li, J. Wu, Z. Wang, Y. Jin, *Ind. Eng. Chem. Res.*, 2023, 62, 16236-16245.
- 2 Z.-L. He, C. Yuan, H. Gao, Z. Mou, S. Qian, C. Zhai and C. Lu, *ACS Sustainable Chem. Eng.*, 2020, 8, 12331-12341.
- 3 K. Zhang, C. Wang, H. You, B. Zou, S. Guo, S. Li and Y. Du, *Chem. Eng. J.*, 2022, 438, 135666.
- 4 K. Zhang, C. Wang, S. Guo, S. Li, Z. Wu, S. Hata, J. Li, Y. Shiraishi and Y. Du, *J. Colloid Interface Sci.*, 2023, 636, 559-567.
- 5 Y. Zhan, W. Hou, G. Li, Y. Shen, Y. Zhang and Y. Tang, *ACS Sustainable Chem. Eng.*, 2019, 7, 17559–17564.
- 6 H. Shi, X. G. Yin, B. Subramaniam and R. V. Chaudhari, *Ind. Eng. Chem. Res.*, 2019, 58, 18561-18568.
- 7 H. Yan, M. Zhao, X. Feng, S. Zhao, X. Zhou, S. Li, M. Zha, F. Meng, X. Chen, Y. Liu, D. Chen, N. Yan and C. Yang, *Angew. Chem.Int. Ed.*, 2022, 61, e202116059.
- 8 H. Yan, S. Yao, J. Wang, S. Zhao, Y. Sun, M. Liu, X. Zhou, G. Zhang, X. Jin, X. Feng, Y. Liu, X. Chen, D. Chen and C. Yang, *Appl. Catal. B.*, 2021, 284, 119803.
- 9 Z. Ren, Y. Li, L. Yu, W. Wang, Y. Yang and M. Wei, *Chem. Eng. J.*, 2023, 468, 143623.
- 10 Z. An, Z. Zhang, Z. Huang, H. Han, B. Song, J. Zhang, Q. Ping, Y. Zhu, H. Song and B. Wang, *Nat. Commun.*, 2022, 13, 5467.
- 11 P. Yang, J. Pan, Y. Liu, X. Zhang, J. Feng, S. Hong and D. Li, *ACS Catal.*, 2018, 9, 188-199.
- 12 M. Gao, P. Yang, X. Zhang, Y. Zhang, D. Li and J. Feng, *Fundam. Res.*, 2022, 2, 412-421.
- 13 X. Zhang, M. Gao, P. Yang, X. Cui, Y. Liu, D. Li and J. Feng, *J. Porous Mater.*, 2021, 28, 1371-1385.
- 14 V. K. Landge, S. H. Sonawane, R. V. Chaudhari and G. U. B. Babu, *Ind. Eng. Chem. Res.*, 2020, 60, 185-195.
- 15 X.-F Zhang, Z. Wang, Y. Zhong, J. Qiu, X. Zhang, X. Gu, J. Yao, *J. Phys. Chem. Solids*. 2019, 126, 27-32.
- 16 W. Yang, J. Zhao, H. Tian, L. Wang, X. Wang, S. Ye, J. Liu, J. Huang, *Small*. 2020, 16, 2002236.
- 17 F. Du, Z. You, K. Meng, X. Qu, D. Zhang, W. Zhang, M. Liu, Y. Shen, W. Deng, X. Jin, *ACS Sustainable Chem. Eng.*, 2021, 9, 14416-14429.
- 18 R. Cao, T. Xia, R. Zhu, Z. Liu, J. Guo, G. Chang, Z. Zhang, X. Liu, Y. He, *Appl. Surf. Sci.* 2018, 433, 840-846.
- 19 S.-Y Ding, E.-M You, Z.-Q Tian, M. Moskovits, *Chem. Soc. Rev.* 2017,46,4042-4076.